ACS Catalysis

Research Article

pubs.acs.org/acscatalysis

Operando Synthesis of Macroporous Molybdenum Diselenide Films for Electrocatalysis of the Hydrogen-Evolution Reaction

Fadl H. Saadi,[†,‡] Azhar I. Carim,[§] Jesus M. Velazquez,[‡,§] Jack H. Baricuatro,[‡,§] Charles C. L. McCrory,[‡,§] Manuel P. Soriaga,*[,‡,#] and Nathan S. Lewis*[,‡,§,∥,⊥]

[†]Division of Engineering and Applied Sciences, [‡]Joint Center for Artificial Photosynthesis, [§]Division of Chemistry and Chemical Engineering, [∥]Beckman Institute, and [⊥]Kavli Nanoscience Institute, California Institute of Technology, Pasadena, California 91125, United States

[#]Department of Chemistry, Texas A&M University, College Station, Texas 77843, United States

Supporting Information

ABSTRACT: The catalytically inactive components of a film have been converted, through an *operando* method of synthesis, to produce a catalyst for the reaction that the film is catalyzing. Specifically, thin films of molybdenum diselenide have been synthesized using a two-step wet-chemical method, in which excess sodium selenide was first added to a solution of ammonium heptamolydbate in aqueous sulfuric acid, resulting in the spontaneous formation of a black precipitate that contained molybdenum triselenide ($MoSe_3$), molybdenum trioxide (MoO_3), and elemental selenium. After purification and after the film had been drop cast onto a glassy carbon electrode, a reductive potential was applied to the precipitate-coated electrode. Hydrogen evolution occurred within the range of potentials applied to the electrode, but during the initial voltammetric cycle, an overpotential of ∼400 mV was required to drive the hydrogen-evolution reaction at a benchmark current density of −10 mA cm^{-2}. The overpotential required to evolve hydrogen at the benchmark rate progressively decreased with subsequent voltammetry cycles, until a steady state was reached at which only ∼250 mV of overpotential was required to pass −10 mA cm^{-2} of current density. During the electrocatalysis, the catalytically inactive components in the as-prepared film were (reductively) converted to $MoSe_2$ through an *operando* method of synthesis of the hydrogen-evolution catalyst. The initial film prepared from the precipitate was smooth, but the converted film was completely covered with pores ∼200 nm in diameter. The porous $MoSe_2$ film was stable while being assessed by cyclic voltammetry for 48 h, and the overpotential required to sustain 10 mA cm^{-2} of hydrogen evolution increased by <50 mV over this period of operation.

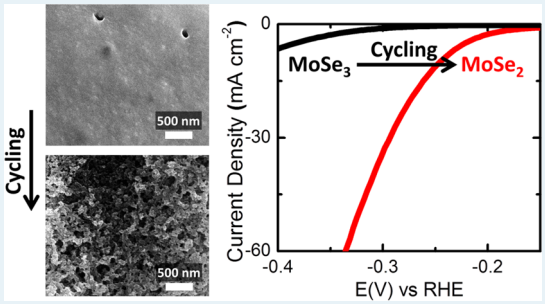

KEYWORDS: *hydrogen-evolution reaction, synthesis of molybdenum diselenide, wet-chemical synthesis of layered electrocatalysts, mesoporous catalysts, synthesis of group VI dichalcogenides*

INTRODUCTION

The ability to generate H_2(g) and O_2(g) by efficiently splitting water would allow the realization of many developmental designs for renewable energy technologies.[1−4] Although the free energy change required to split one molecule of water corresponds to a ΔE° of 1.23 V per electron transferred, the electrolysis of water typically requires the application of an overpotential to drive the kinetically rate-liming steps involved with the multistep oxidation and reduction half-reactions.[4] Catalysts can improve the kinetics and efficiencies of the cathodic [hydrogen-evolution reaction (HER)] and anodic [oxygen-evolution reaction (OER)] half-reactions. At present, the most efficient water-splitting catalysts contain scarce metals like platinum (for the HER)[4−8] and iridium (for the OER).[4] The discovery of active HER and OER catalysts made from earth-abundant elements would therefore constitute a key step in the development of a globally scalable water-splitting technology.

Catalysis of the HER has been demonstrated using catalysts made from earth-abundant elements such as nickel alloys.[9−13] In particular, nickel−molybdenum alloys require the application of only ∼50 mV of overpotential to catalyze the HER at a current density of −10 mA cm^{-2}.[10−16] However, nickel−molybdenum alloys are unstable in strongly acidic solutions,[10,17] where proton-exchange membranes are operational and where the voltage loss due to the formation of a pH gradient across the membrane can be minimized.[17,18]

Recently, materials such as Ni_2P, CoSe, and group VI chalcogenides have been classified as catalytic for the hydrogen-evolution reaction and stable in acidic media.[17,19,20] Group VI chalcogenides such as molybdenum disulfide (MoS_2), molybdenum diselenide ($MoSe_2$), tungsten disulfide (WS_2), and

Received: December 16, 2013
Revised: July 17, 2014
Published: July 17, 2014

tungsten diselenide (WSe_2) are comprised of earth-abundant elements, are stable in strong acid, and catalyze the HER with reported overpotentials of ~200−350 mV to produce current densities of −10 mA cm^{-2}.[7,14,19,21−42] Theoretical[22,30] and experimental[19] studies of MoS_2 crystals suggest that the $\langle 10\bar{1}0 \rangle$ edge sites are the active sites for hydrogen evolution. Many methods of preparing catalytically active MoS_2 have been developed, including sulfurization of molybdenum,[37] electrochemical deposition from ammonium thiomolybdate,[6,40] wet-chemical techniques,[24] and *ex crystallum* mechanical exfoliation.[35,43] In contrast, relatively few methods of preparing catalytically active $MoSe_2$, such as the selenization of metallic molybdenum, have been disclosed.[37,38]

We describe a two-step method for the synthesis of $MoSe_2$ films that are stable in acid and capable of catalyzing the HER. This method extends to $MoSe_2$ a synthetic route that has been reported for MoS_2.[24,27] In the first step, wet-chemical techniques are used to form a mixed-composition precipitate, which is then deposited as a film onto electrodes. The film-covered electrodes are then introduced into aqueous acid and used to drive the HER. The as-prepared films exhibited low catalytic activity, but the activity improved under the conditions of the HER, which convert the mixed-composition film into a macroporous film of $MoSe_2$. The synthesis can be categorized as *operando* because the $MoSe_2$ catalyst is produced under the conditions of the reaction that it catalyzes.

EXPERIMENTAL SECTION

All chemicals and materials were used as received, and all experiments were performed under ambient laboratory conditions, except where otherwise noted. Water was obtained from a Barnstead Nanopure purification system (Thermo Scientific, Asheville, NC) and had a resistivity ≥18.2 MΩ cm. All glassware was thoroughly cleaned in hot chromic acid (3% potassium dichromate in 10 M H_2SO_4).

Mixed-Composition Suspension. Ammonium heptamolybdate, $(NH_4)_6Mo_7O_{24}\cdot 4H_2O$ [0.60 g, 5.2×10^{-4} mol, 99.98% (Sigma-Aldrich, St. Louis, MO)], was dissolved in 12 mL of a 0.20 M H_2SO_4 solution prepared by diluting 18 M H_2SO_4 (Sigma-Aldrich) with H_2O. A separate solution was prepared by dissolving 0.15 g (1.2×10^{-3} mol) of sodium selenide, Na_2Se [99.8% (Alfa Aesar, Ward Hill, MA)], in 12 mL of H_2O. Inside a fume hood, the first solution was quickly poured into the second solution, and a black precipitate formed upon mixing.

The suspension was transferred to a centrifuge tube and centrifuged at 12000 rpm for 30 min using a JA-17 rotor (Beckman Coulter, Brea, CA). A black precipitate collected at the bottom of the centrifuge tube. The yield was calculated to be 70%. The clear supernatant liquid was discarded, and the precipitate was rinsed with several 15 mL aliquots of 2-propanol [99.7% (Macron Chemicals, Center Valley, PA)]. A final 15 mL of 2-propanol was then added to the centrifuge tube, which was then subjected to sonication for 30 min. This process resulted in suspension of the black solid in the 2-propanol.

Preparation of Film-Coated Rotating-Disk Electrodes (RDEs). Glassy carbon disks (HTW Hochtemperatur-Werkstoff GmbH, Thierhaupten, Germany), 5 mm in diameter and 4 mm in thickness, were polished on a LaboPol-5 polishing wheel (Struers, Inc., Cleveland, OH), first with a 600 grit Carbimet SiC grinding paper (Buehler, Lake Bluff, IL) for 30 s and subsequently with diamond slurries (Buehler) with diamond particle sizes of 9, 6, 3, 1, and 0.1 μm, also for 30 s each. The carbon disks were then cleaned by being sonicated for 5 min *seriatim* in 2-propanol (Macron Chemicals), acetone (ACS grade, Sigma-Aldrich), and water.

A 30 μL drop (mass loading of 1.36 mg cm^{-2}) of the mixed-composition suspension was placed onto the polished side of a glassy carbon disk. The disk was then dried for 12 h in a vacuum desiccator with an internal pressure of 5000 Pa (50 mbar).

Electrochemistry. A 0.10 M solution of H_2SO_4 was used as the electrolyte for electrochemical experiments. A 250 mL four-port glass cell was filled with the electrolyte and equipped with a film-coated rotating-disk electrode (RDE), a graphite rod [99% pure (Alfa Aesar)] that served as a counter electrode, and a Ag/AgCl reference electrode (CH Instruments, Austin, TX). The Ag/AgCl electrode consisted of a Ag wire in 1.0 M KCl and had been calibrated against a reversible hydrogen electrode (RHE) prior to use in these experiments, with the Ag/AgCl electrode having a potential of 280 ± 2 mV vs the RHE. Potentiostatic control was accomplished using a BioLogic SP-200 potentiostat (Biologic, Grenoble, France). The uncompensated cell resistance was determined from a single-point (100 kHz) high-frequency impedance measurement and was 85% compensated by the BioLogic positive-feedback software. The RDE was rotated at a rate of 1600 rpm during the experiments. During all of the HER-catalysis experiments, the cell was saturated with H_2 [99.999% (Air Liquide, Plumsteadville, PA)] by bubbling the gas through the solution.

Cyclic voltammetric scans were obtained by sweeping the applied voltage between 0.00 and −0.40 V versus the RHE at a scan rate of 5 mV s^{-1}. To evaluate the stability of the films, the cyclic voltammetric scans were performed continuously over a 48 h period. The physical characterization of the films was performed after 10 cycles.

The surface roughness factors for the thin films were calculated from double-layer capacitance measurements.[44−46] Current density versus potential data were acquired by sweeping the applied potential at various scan rates (20, 40, 80, 150, and 300 mV s^{-1}) in a potential range within which no Faradaic electron-transfer processes were observed (0.28−0.38 V vs the RHE). The geometric capacitance of the thin films was calculated as the slope of a plot of the scan rate versus current density at 0.34 V, which is the midpoint potential of the non-Faradaic region. The surface roughness factors for the thin films were calculated by dividing the measured geometric capacitance by the specific capacitance of MoS_2, which was taken to be 60 μF cm^{-2}.[21,44−46]

Scanning Electron Microscopy. Scanning electron micrographs were acquired with an FEI Nova electron microscope (FEI, Hillsboro, OR) at a working distance of 5.0 mm. Low-magnification micrographs (field width of >100 μm) were obtained at an accelerating voltage of 10 kV with an Everhart-Thornley detector, whereas higher-magnification experiments utilized an accelerating voltage of 15 kV and a through-the-lens detector.

X-ray Photoelectron Spectroscopy. X-ray photoelectron spectroscopy (XPS) data for elemental composition and valence information were collected with an Axis Ultra X-ray photoelectron spectrometer (Kratos, Manchester, U.K.) at a base pressure of $<10^{-9}$ Torr. Data were obtained with a monochromatic Al Kα source (1486.7 eV) and a concentric hemispherical analyzer with a pass energy of 20 eV, with the photoelectrons captured normal to the surface. Binding energies were calibrated against the "adventitious" C 1s peak

dx.doi.org/10.1021/cs500412u | ACS Catal. 2014, 4, 2866−2873

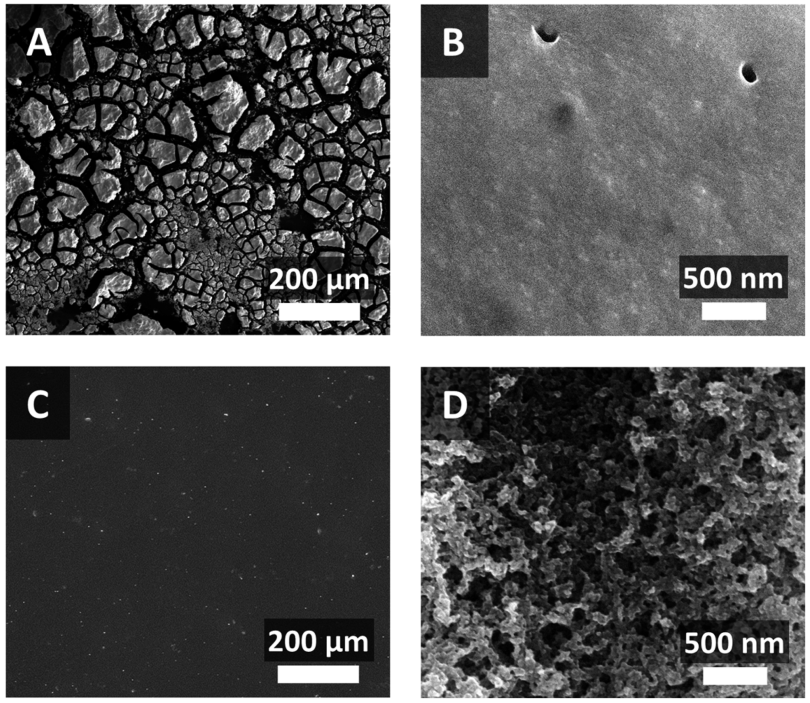

Figure 1. Scanning electron micrographs of the films before (A and B) and after (C and D) 10 voltammetric cycles. (A) The as-deposited mixed-composition films on glassy carbon substrates were nonuniform, consisting of multiple islands ~100 μm in diameter. (B) The surfaces of the islands were relatively smooth. (C) The island structure was not visible after electrocatalysis. (D) At a higher magnification, the entire surface appeared to be porous.

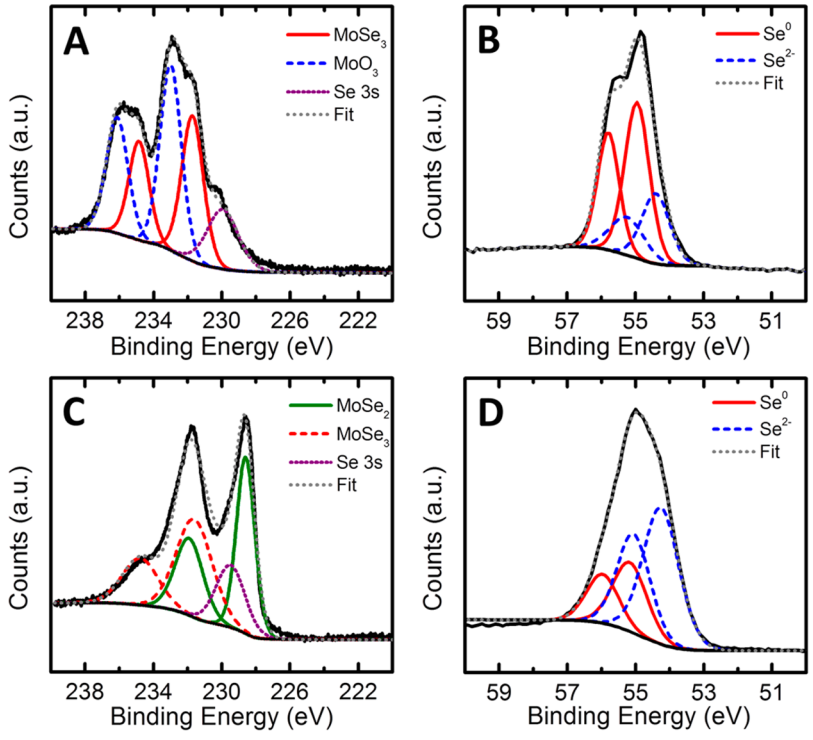

Figure 2. High-resolution X-ray photoelectron spectra of (A) the Mo 3d region of an as-deposited thin film, (B) the Se 3d region of an as-deposited thin film, (C) the Mo 3d region after 10 voltammetric cycles, and (D) the Se 3d region after 10 cycles.

(taken to be 284.65 eV). Peak fitting was performed using CasaXPS (CASA Ltd., Teignmouth, U.K.) assuming a Shirley background[47] and symmetric Voigt line shapes comprised of Gaussian (70%) and Lorentzian (30%) functions. Peak fitting was constrained to maintain a 2:3 ratio between the areas of the Mo $3d_{3/2}$ and Mo $3d_{5/2}$ peaks and to maintain a 3.15 eV separation between the binding energies of those two peaks. The possibility of Se existing in the bridging Se_2^{2-} form, analogous to what has been reported for S in MoS_3,[27] was not considered here in the interpretation of the Se XPS spectra.

dx.doi.org/10.1021/cs500412u | ACS Catal. 2014, 4, 2866−2873

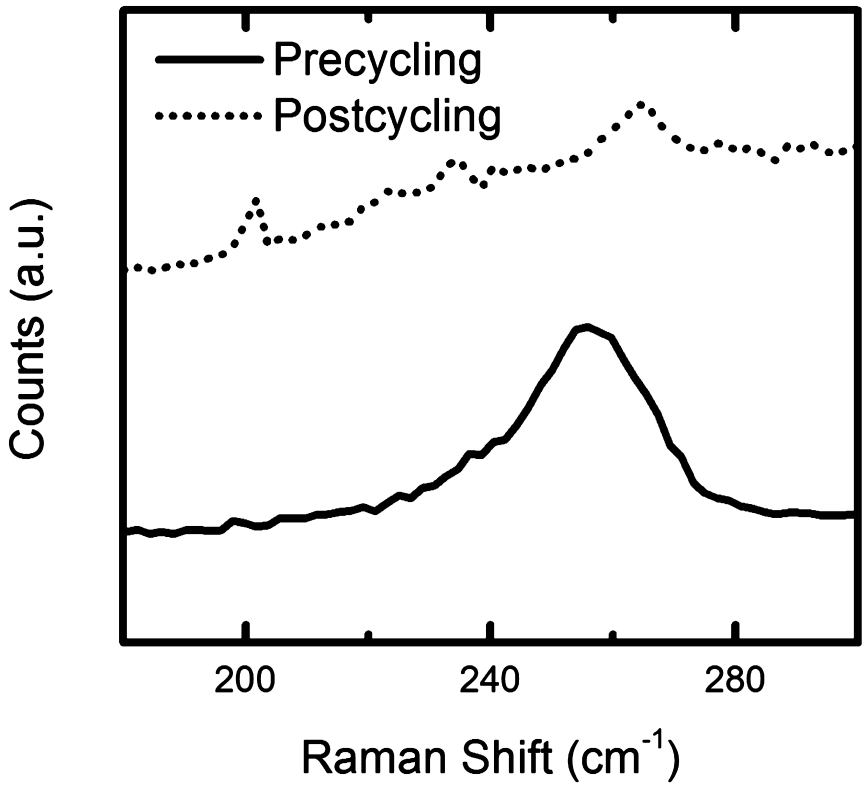

Figure 3. Raman spectra of an as-deposited thin film (—) and of a film after 10 voltammetric cycles (···). Prior to voltammetric cycling, a broad, asymmetric band centered at 255 cm^{-1} and a smaller shoulder at 238 cm^{-1} were visible and were assigned to a Se−Se stretch mode in glassy, loosely packed polymer chains and to a Se−Se stretch vibration of closely packed chains, respectively. These bands were not observed after voltammetric cycling.

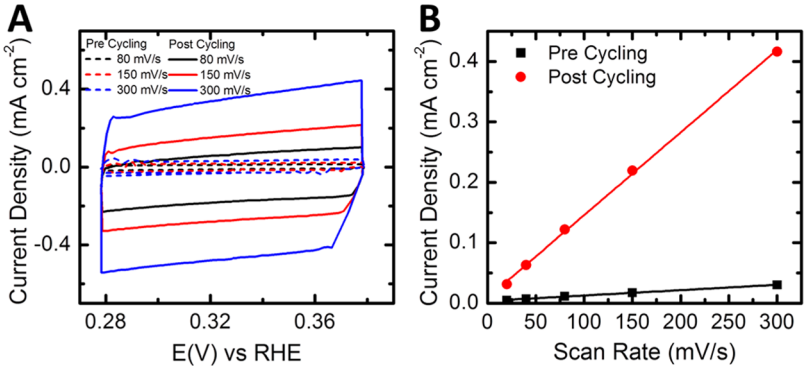

Figure 4. Electrochemically active surface area measurements before (precycling) and after (postcycling) the electrocatalysis experiments shown in Figure 5. (A) Cyclic nonfaradaic current vs potential curves at preselected scan rates. (B) Nonfaradaic current as a function of the potential scan rate.

Raman Spectroscopy. Raman spectra of the films were recorded with a Renishaw inVia Raman microprobe (Renishaw, Wotton Under Edge, U.K.) equipped with a Leica DM 2500M microscope, a Leica N Plan 50× objective (Leica, Wetzlar, Germany) (numerical aperture of 0.75), a 1800 lines/mm grating, and a CCD detector configured in a 180° backscatter geometry. A 532 nm diode-pumped solid-state laser (Renishaw model RL532C50) was used as the excitation source and delivered a 20 μW radiant flux at the surface of the sample.

RESULTS

Characterization of As-Deposited Films. Panels A and B of Figure 1 show scanning electron micrographs (SEMs) of a mixed-composition film on a glassy carbon substrate. The deposition was nonuniform and consisted of multiple islands ~100 μm in diameter separated by crevices up to 50 μm in width. Each island, however, was smooth and nonporous.

Panels A and B of Figure 2 present high-resolution composite XPS spectra of the samples in the Mo and Se regions. Two sets of doublet peaks for Mo were observed (Figure 2A). The first doublet consisted of signals for Mo $3d_{5/2}$ at 233 eV and Mo $3d_{3/2}$ at 236 eV and is characteristic of MoO_3.[23,48] The second doublet consisted of peaks for Mo $3d_{5/2}$ at 232 eV and Mo $3d_{3/2}$ at 235 eV and was located in a region typically associated with Mo^{6+}.[49] The single peak at 230 eV is characteristic of Se 3s. Figure 2B displays the Se region with two sets of 3d doublets: the higher-energy doublet that can be ascribed to Se^0 and the lower-energy doublet that can be ascribed to Se^{2-}.[50,51] Quantitation of the Mo $3d_{5/2}$ peak at 232 eV and the Se^{2-} 3d peak at 54 eV yields a Mo:Se ratio of 1:3.

dx.doi.org/10.1021/cs500412u | ACS Catal. 2014, 4, 2866−2873

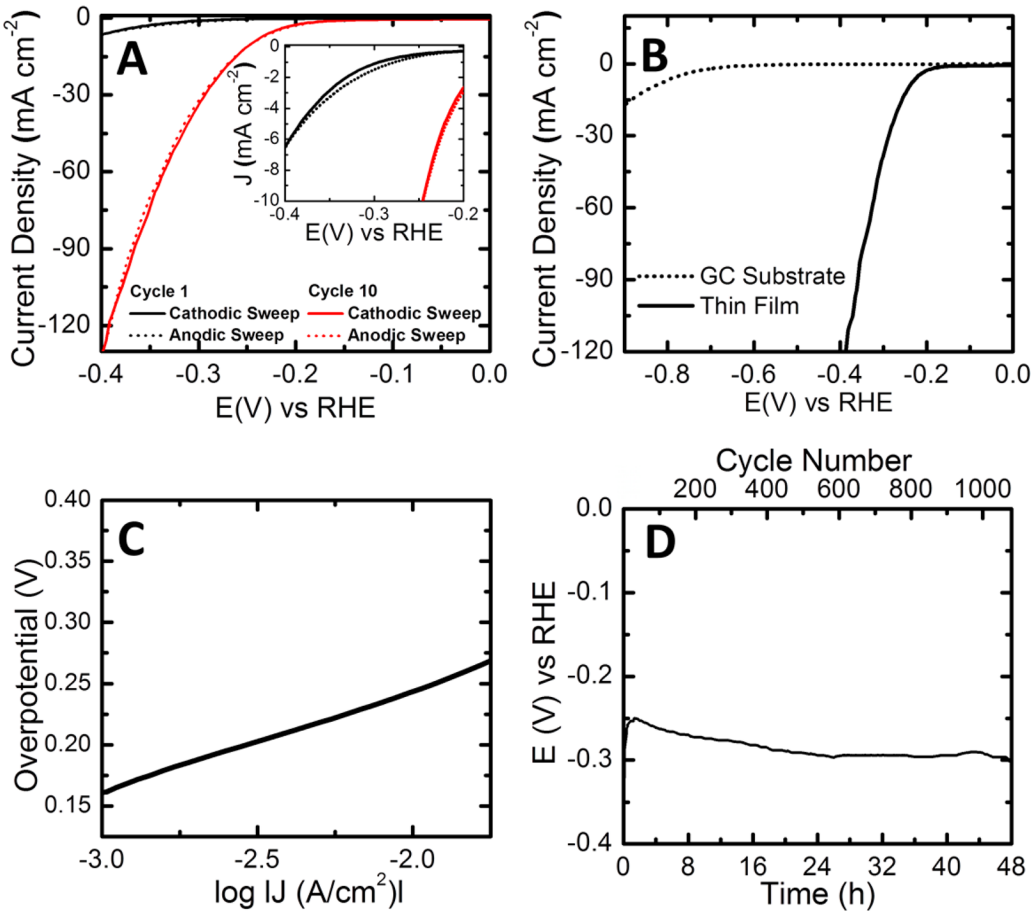

Figure 5. (A) Cyclic voltammetric data for molybdenum selenide thin films on glassy carbon in 0.10 M H_2SO_4(aq). In the first cycle, the initial cathodic portion showed a current density lower than that of the return anodic half-cycle. The current density increases in subsequent cycles, until the 10th cycle when the current density reached a steady state. (B) Current−potential plot for the glassy carbon substrate (···) and immediately after the 10th (—) cycle. (C) Tafel plot of the current−potential data in panel B. (D) Plot of the overpotential needed to produce a current density of 10 mA cm^{-2} as a function of time.

The Raman spectrum of the as-deposited thin film exhibited a broad, asymmetric band centered at 255 cm^{-1} and a shoulder at ∼238 cm^{-1} (Figure 3). The prominent, higher-frequency peak is characteristic of a Se−Se stretch mode in glassy, loosely packed polymer chains, whereas the lower-energy shoulder is also due to a Se−Se stretch vibration but indicates closely packed chains in which the local microscopic structure resembles that of crystalline (trigonal) Se.[52]

Figure 4 shows the current density versus scan rate data that were used to calculate the geometric capacitance of a typical mixed-composition thin film. The geometric capacitance of the film was 120 μF cm^{-2}, and the roughness factor of the film was ∼2.

Conversion of the Films to Catalysts of the HER. Figure 5A shows the first and 10th cyclic voltammetric cycles obtained using the film-coated glassy carbon RDEs. The onset of hydrogen evolution clearly shifted to less negative potentials between the first and 10th cycles. A steady state was reached by the 10th cycle, at which point 250 mV of overpotential was needed to produce a current density of −10 mA cm^{-2}. On the basis of the steady-state negative potential sweep data illustrated in Figure 5B, the Tafel slope was determined to be 80 mV dec^{-1} with an exchange current density of 1×10^{-5} mA cm^{-2} (Figure 5C).

The stability of the prepared film was characterized by plotting the overpotential required to produce a current density of 10 mA cm^{-2} for each cyclic voltammetric sweep performed for 48 h. As shown in Figure 5D, the overpotential to produce −10 mA cm^{-2} for the HER increased by ∼50 mV over a 48 h operation.

Characterization of Converted Films. Panels C and D of Figure 1 show SEMs after reductive conversion of the films to HER catalysts during the electrochemical experiments. Substantial changes to the surface terrain were evident relative to the terrain in the pre-electrochemistry micrographs (Figure 1A,B). The island structures that were prominent at low levels of magnification prior to conversion of the films were no longer visible, and the film appeared to be smooth. However, a macroporous structure that was absent prior to conversion of the films was apparent at higher-magnification levels and covered the entire sample. The pore sizes were estimated to be ∼200 nm in diameter.

The high-resolution X-ray photoelectron spectra of the Mo 3d and Se 3d regions for the converted films are displayed in panels C and D of Figure 2. The Se 3s signal at 230 eV remained unchanged from that of the preconversion spectra, but the rest of the peak profile in Figure 2C was clearly different after the electrochemistry. The intensities of the Mo^{6+} doublet at 232 and 235 eV were significantly reduced, and the Mo^{4+}

dx.doi.org/10.1021/cs500412u | ACS Catal. 2014, 4, 2866−2873

doublet[50] predominated the spectrum at 228.6 and 232 eV. More significantly, the Mo^{6+} peaks ascribed to MoO_3 were extinguished after electrolysis. The Se^{2-} species in Figure 2D were, therefore, associated with both Mo^{4+} and Mo^{6+} species in the form of $MoSe_2$ and $MoSe_3$. The magnitude of the Se^0 doublet, which was prominent in the preconversion spectra (Figure 2B), decreased significantly after electrolysis, whereas the magnitude of the doublet attributed to Se^{2-} increased. The Mo_{total}:Se^{2-} ratio after electrolysis was found to be 1:2.2. A definitive quantitative assignment of the stoichiometric portion of the Se^{2-} that belongs to $MoSe_2$ and $MoSe_3$ necessitates a mass balance study of Se, which is not within the purview of this work.

It is important to note that, before electrolysis, the O 1s peak (Figure S9 of the Supporting Information) appeared at 530.7 eV; the same O 1s peak was observed for both the oxided molybdenum standards, MoO_3 (Figure S7 of the Supporting Information) and MoO_2 (Figure S8 of the Supporting Information). After electrolysis, the O 1s peak shifted positively to 532 eV, implying the presence of adventitious oxygen, not of oxygen associated with oxided molybdenum species.

The Raman spectrum also exhibited significant changes after electrochemical conversion of the films (Figure 3). The vibrational band centered at ~255 cm^{-1}, which was prominent in the as-prepared films, was not observed for the converted films, suggesting that the amorphous polymeric chains of elemental Se were removed from the film during the reductive conversion process. No vibrational peaks characteristic of crystalline molybdenum selenide were detected for the converted films, suggesting that the films remained noncrystalline.

Figure 4 shows the current density versus scan rate data used to calculate the geometric capacitance of the converted films. The geometric capacitance of the film was 1200 $\mu F\ cm^{-2}$, and the roughness factor of the film was ~20, an order of magnitude larger than that measured in the as-deposited thin film.

DISCUSSION

Reaction pathways directly analogous to those reported previously[53−55] for MoS_2 likely apply to the wet-chemical synthesis of the mixed-composition precipitate. In aqueous solutions, ammonium heptamolybdate, $(NH_4)_6Mo_7O_{24}{\cdot}H_2O$, exists as ammonium orthomolybdate, $(NH_4)_2MoO_4$, a strong electrolyte.[56] Mo is hexavalent in both of these structures. Hence, when sodium selenide is added to an acidic solution of $(NH_4)_6Mo_7O_{24}{\cdot}H_2O$, the reaction that generates the black precipitate is likely to be

$$MoO_4^{2-} + 3H_2Se \rightarrow MoSe_3 + 2OH^- + 2H_2O \quad (1)$$

where $MoSe_3$ is the black solid. The XPS data (Figure 2A,B) support the presence of Mo^{6+} and Se^{2-} in the as-prepared films. The same set of XPS data also indicates the presence of MoO_3, which may be formed either under the synthesis conditions presented here or by exposure of the synthesized $MoSe_3$ to air:

$$2MoSe_3 + 3O_2 \rightarrow 2MoO_3 + 6Se \quad (2)$$

Equation 1 may also be accompanied, to a small extent, by the decomposition of $MoSe_3$:

$$MoSe_3 \rightarrow MoSe_2 + Se \quad (3)$$

The Se produced from reactions 2 and 3 was detected by XPS and Raman spectroscopy.

$MoSe_2$, which is believed to be an active catalyst for the HER, is present only at very low concentrations, if at all, in the unconverted films, which consist of a mixture of $MoSe_3$, MoO_3, and Se. The as-prepared films are therefore relatively inactive HER catalysts. Reductive cycling significantly improved the catalytic activity of the films (Figure 5A), and a steady state was achieved after 10 voltammetric cycles. This behavior is consistent with a process in which exposure of the multicomponent film to negative potentials, and consequent reductive generation of $H_2(g)$, also served to concentrate $MoSe_2$, based on a combination of three interfacial reactions that are analogous to the known reactions of MoS_2 and H_2S:[53,57,58]

$$H_2 + Se \rightarrow H_2Se \quad (4)$$

$$MoSe_3 + H_2 \rightarrow MoSe_2 + H_2Se \quad (5)$$

$$MoO_3 + 3H_2Se \rightarrow MoSe_2 + 3H_2O + Se \quad (6)$$

These reaction schemes are supported by the postelectrochemistry surface analysis. (i) The XPS results (Figure 2C,D) showed a decrease in the magnitudes of the MoO_3 and $MoSe_3$ peaks and an emergence of the $MoSe_2$ signal, and (ii) the Raman spectrum (Figure 3) did not exhibit the vibrational mode for amorphous elemental Se.

The observed increase in the porosity and surface area of the film (Figure 4) may be due to several factors such as the expulsion of gases like H_2 and H_2Se. The release of H_2Se, represented in reaction 4, is analogous to the formation of H_2S that accompanies the reduction of MoS_3 to MoS_2;[59,60] hence, the decrease in the C:Se mole ratio (Table S1 of the Supporting Information) after the reductive conversion is not unexpected as the prepared material loses part of its selenium during potential cycling. Material loss due to the dissolution of MoO_3 also could contribute to the observed porosity. Approximately 50% of the as-prepared film was clearly lost after electrolysis, which can be gleaned from the decline in atomic abundances of both Mo and Se (Table S1 of the Supporting Information) normalized with respect to the atomic abundance of C.

Figure S1 of the Supporting Information plots the current divided by the electrochemically active surface area versus potential of the samples before and after 10 voltammetric cycles. Notably, the improvement in the catalytic activity of the material cannot be attributed solely to the increase in the internal surface area of the film; i.e., the catalytic activity of the film was still superior after voltammetry even when the increase in the electrochemically active surface area had been accounted for.

The overpotential for the onset for hydrogen evolution was measured to be ~150 mV (Figure 5A). The overpotential necessary to effect a HER current density of −10 mA cm^{-2}, a heuristic benchmark for assessing catalytic activity in solar fuel applications under unconcentrated sunlight, was <250 mV (Figure 5B) and is within the range that has been reported for MoS_2 HER catalysts (~200−350 mV).[6,23−25,27,28,37] The porous $MoSe_2$ films had a catalytic activity higher than and a Tafel slope lower than those of thin films of $MoSe_2$ synthesized via the selenization of Mo on glassy carbon, which required an overpotential of 430 mV to achieve a current density of −8 mA cm^{-2} and reported a Tafel slope of 105−120 mV dec^{-1} and stability for >1000 cycles.[37,38]

dx.doi.org/10.1021/cs500412u | ACS Catal. 2014, 4, 2866−2873

Although Faradaic yields have not been determined directly, competing cathodic processes are unlikely. Stoichiometric reactions involving Mo or Se cannot have contributed more than 1% to the charge passed during a 24 h chronoamperometric experiment (cf., Supporting Information). In a thermoelectrochemical process, electroreduction of H_2SO_4 to H_2S has been shown to occur at moderate potentials in the absence of H_2 gas but requires elevated temperatures ($T \geq 120$ °C), high acidity ($C_{H_2SO_4} \geq 6.5$ M), and the use of graphitic carbon electrodes.[61]

The macroporous $MoSe_2$ thin films were stable catalysts of the HER in acidic media, and the overpotential required to sustain a current density of −10 mA cm^{-2} increased by only 50 mV over 48 h. Although a comparison of stability across catalysts is not straightforward, because of the wide range of results that have been reported, the macroporous thin film $MoSe_2$ catalysts appear to be at least as stable over the same time period as MoS_2 HER catalysts.[24]

CONCLUSION

The catalytically inactive components of a $MoSe_3/MoO_3$ film have been converted, through an *operando* method of synthesis, to produce a catalyst for the HER while the film is catalyzing the HER. The addition of excess sodium selenide to ammonium heptamolydbate in aqueous sulfuric acid resulted in the spontaneous formation of a black precipitate that consisted primarily of molybdenum triselenide ($MoSe_3$) with small amounts of elemental Se. Molybdenum trioxide (MoO_3) was also formed upon exposure of the triselenide to atmospheric oxygen. The multicomponent thin film cast onto glassy carbon was relatively inactive for the HER during initial voltammetric cycles, because the active catalyst, $MoSe_2$, was not present or was present only at very low concentrations. Further voltammetric cycling of the electrode in the potential region where the HER occurs led to substantial increases in catalytic activity. By the 10th cycle, the overpotential needed to drive a catalytic current of −10 mA cm^{-2} had decreased from ∼450 to 250 mV. The improvement in the catalytic activity occurred because, under HER conditions, the catalytically inactive components of the film were reductively converted to $MoSe_2$. An *operando* synthesis of $MoSe_2$ was thus established. An amorphous, macroporous $MoSe_2$ framework was also generated in the synthesis, and the $MoSe_2$ film exhibited long-term stability with an only 50 mV increase in overpotential after continuous operation for 48 h. The porous $MoSe_2$ films appear to hold promise as a catalyst for the HER in aqueous acidic electrolytes.

ASSOCIATED CONTENT

Supporting Information

Current density normalized to the electrochemical active surface area, transmission electron microscopy and XRD of samples before electrolysis, Raman and XPS of single-crystal $MoSe_2$, and XPS of MoO_3 and MoO_2. This material is available free of charge via the Internet at http://pubs.acs.org.

AUTHOR INFORMATION

Corresponding Authors

*E-mail: m-soriaga@tamu.edu.
*E-mail: nslewis@caltech.edu.

Notes

The authors declare no competing financial interest.

ACKNOWLEDGMENTS

This material is based upon work performed by the Joint Center for Artificial Photosynthesis, a U.S. Department of Energy (DOE) Energy Innovation Hub, supported through the Office of Science of the DOE via Grant DE-SC0004993. A.I.C. acknowledges a National Science Foundation Graduate Research Fellowship for support.

REFERENCES

(1) Turner, J.; Sverdrup, G.; Mann, M. K.; Maness, P.-C.; Kroposki, B.; Ghirardi, M.; Evans, R. J.; Blake, D. *Int. J. Energy Res.* **2008**, *32*, 379−407.
(2) Lewis, N. S.; Nocera, D. G. *Proc. Natl. Acad. Sci. U.S.A.* **2006**, *103*, 15729−15735.
(3) Lewis, N. S. *Science* **2007**, *315*, 798−801.
(4) Walter, M. G.; Warren, E. L.; McKone, J. R.; Boettcher, S. W.; Mi, Q.; Santori, E. A.; Lewis, N. S. *Chem. Rev.* **2010**, *110*, 6446−6473.
(5) Gray, H. B. *Nat. Chem.* **2009**, *1*, 7.
(6) Merki, D.; Hu, X. *Energy Environ. Sci.* **2011**, *4*, 3878−3888.
(7) Laursen, A. B.; Kegnæs, S.; Dahl, S.; Chorkendorff, I. *Energy Environ. Sci.* **2012**, *5*, 5577−5591.
(8) Bak, T.; Nowotny, J.; Rekas, M.; Sorrell, C. C. *Int. J. Hydrogen Energy* **2002**, *27*, 991−1022.
(9) Paseka, I. *Electrochim. Acta* **1995**, *40*, 1633−1640.
(10) McKone, J. R.; Sadtler, B. F.; Werlang, C. A.; Lewis, N. S.; Gray, H. B. *ACS Catal.* **2013**, *3*, 166−169.
(11) Brown, D. E.; Mahmood, M. N.; Man, M. C. M.; Turner, A. K. *Electrochim. Acta* **1984**, *29*, 1551−1556.
(12) Brown, D. E.; Mahmood, M. N.; Turner, A. K.; Hall, S. M.; Fogarty, P. O. *Int. J. Hydrogen Energy* **1982**, *7*, 405−410.
(13) Raj, I. A.; Vasu, K. I. *J. Appl. Electrochem.* **1990**, *20*, 32−38.
(14) Merki, D.; Fierro, S.; Vrubel, H.; Hu, X. *Chem. Sci.* **2011**, *2*, 1262−1267.
(15) Krstajić, N. V.; Jović, V. D.; Gajić-Krstajić, L.; Jović, B. M.; Antozzi, A. L.; Martelli, G. N. *Int. J. Hydrogen Energy* **2008**, *33*, 3676−3687.
(16) McKone, J. R.; Warren, E. L.; Bierman, M. J.; Boettcher, S. W.; Brunschwig, B. S.; Lewis, N. S.; Gray, H. B. *Energy Environ. Sci.* **2011**, *4*, 3573−3583.
(17) Popczun, E. J.; McKone, J. R.; Read, C. G.; Biacchi, A. J.; Wiltrout, A. M.; Lewis, N. S.; Schaak, R. E. *J. Am. Chem. Soc.* **2013**, *135*, 9267−9270.
(18) Hernandez-Pagan, E. A.; Vargas-Barbosa, N. M.; Wang, T.; Zhao, Y.; Smotkin, E. S.; Mallouk, T. E. *Energy Environ. Sci.* **2012**, *5*, 7582−7589.
(19) Jaramillo, T. F.; Jorgensen, K. P.; Bonde, J.; Nielsen, J. H.; Horch, S.; Chorkendorff, I. *Science* **2007**, *317*, 100−102.
(20) Carim, A. I.; Saadi, F. H.; Soriaga, M. P.; Lewis, N. S. *J. Mater. Chem. A* **2014**, DOI: 10.1039/c4ta02611j.
(21) Jaramillo, T. F.; Bonde, J.; Zhang, J.; Ooi, B.-L.; Andersson, K.; Ulstrup, J.; Chorkendorff, I. *J. Phys. Chem. C* **2008**, *112*, 17492−17498.
(22) Bonde, J.; Moses, P. G.; Jaramillo, T. F.; Nørskov, J. K.; Chorkendorff, I. *Faraday Discuss.* **2009**, *140*, 219−231.
(23) Chen, Z.; Cummins, D.; Reinecke, B. N.; Clark, E.; Sunkara, M. K.; Jaramillo, T. F. *Nano Lett.* **2011**, *11*, 4168−4175.
(24) Benck, J. D.; Chen, Z.; Kuritzky, L. Y.; Forman, A. J.; Jaramillo, T. F. *ACS Catal.* **2012**, *2*, 1916−1923.
(25) Kibsgaard, J.; Chen, Z.; Reinecke, B. N.; Jaramillo, T. F. *Nat. Mater.* **2012**, *11*, 963−969.
(26) Merki, D.; Vrubel, H.; Rovelli, L.; Fierro, S.; Hu, X. *Chem. Sci.* **2012**, *3*, 2515−2525.
(27) Vrubel, H.; Merki, D.; Hu, X. *Energy Environ. Sci.* **2012**, *5*, 6136−6144.
(28) Vrubel, H.; Hu, X. *ACS Catal.* **2013**, *3*, 2002−2011.
(29) Vrubel, H.; Moehl, T.; Gratzel, M.; Hu, X. *Chem. Commun.* **2013**, *49*, 8985−8987.

(30) Hinnemann, B.; Moses, P. G.; Bonde, J.; Jørgensen, K. P.; Nielsen, J. H.; Horch, S.; Chorkendorff, I.; Nørskov, J. K. *J. Am. Chem. Soc.* **2005**, *127*, 5308−5309.
(31) Nielsen, J. H.; Bech, L.; Nielsen, K.; Tison, Y.; Jørgensen, K. P.; Bonde, J. L.; Horch, S.; Jaramillo, T. F.; Chorkendorff, I. *Surf. Sci.* **2009**, *603*, 1182−1189.
(32) Hou, Y.; Abrams, B. L.; Vesborg, P. C. K.; Björketun, M. E.; Herbst, K.; Bech, L.; Setti, A. M.; Damsgaard, C. D.; Pedersen, T.; Hansen, O.; Rossmeisl, J.; Dahl, S.; Nørskov, J. K.; Chorkendorff, I. *Nat. Mater.* **2011**, *10*, 434−438.
(33) Seger, B.; Laursen, A. B.; Vesborg, P. C. K.; Pedersen, T.; Hansen, O.; Dahl, S.; Chorkendorff, I. *Angew. Chem., Int. Ed.* **2012**, *51*, 9128−9131.
(34) Wu, Z.; Fang, B.; Wang, Z.; Wang, C.; Liu, Z.; Liu, F.; Wang, W.; Alfantazi, A.; Wang, D.; Wilkinson, D. P. *ACS Catal.* **2013**, *3*, 2101−2107.
(35) Lukowski, M. A.; Daniel, A. S.; Meng, F.; Forticaux, A.; Li, L.; Jin, S. *J. Am. Chem. Soc.* **2013**, *135*, 10274−10277.
(36) Li, Y.; Wang, H.; Xie, L.; Liang, Y.; Hong, G.; Dai, H. *J. Am. Chem. Soc.* **2011**, *133*, 7296−7299.
(37) Kong, D.; Wang, H.; Cha, J. J.; Pasta, M.; Koski, K. J.; Yao, J.; Cui, Y. *Nano Lett.* **2013**, *13*, 1341−1347.
(38) Wang, H.; Kong, D.; Johanes, P.; Cha, J. J.; Zheng, G.; Yan, K.; Liu, N.; Cui, Y. *Nano Lett.* **2013**, *13*, 3426−3433.
(39) Chang, Y. H.; Lin, C. T.; Chen, T. Y.; Hsu, C. L.; Lee, Y. H.; Zhang, W.; Wei, K. H.; Li, L. J. *Adv. Mater.* **2013**, *25*, 756−760.
(40) Murugesan, S.; Akkineni, A.; Chou, B. P.; Glaz, M. S.; Vanden Bout, D. A.; Stevenson, K. J. *ACS Nano* **2013**, *7*, 8199−8205.
(41) Tang, M. L.; Grauer, D. C.; Lassalle-Kaiser, B.; Yachandra, V. K.; Amirav, L.; Long, J. R.; Yano, J.; Alivisatos, A. P. *Angew. Chem., Int. Ed.* **2011**, *50*, 10203−10207.
(42) Velazquez, J. M.; Saadi, F. H.; Pieterick, A. P.; Spurgeon, J. M.; Soriaga, M. P.; Brunschwig, B. S.; Lewis, N. S. *J. Electroanal. Chem.* **2014**, *716*, 45−48.
(43) Voiry, D.; Yamaguchi, H.; Li, J.; Silva, R.; Alves, D. C. B.; Fujita, T.; Chen, M.; Asefa, T.; Shenoy, V. B.; Eda, G.; Chhowalla, M. *Nat. Mater.* **2013**, *12*, 850−855.
(44) Trasatti, S.; Petrii, O. A. *Pure Appl. Chem.* **1991**, *63*, 711−734.
(45) Conway, B. E.; Birss, V.; Wojtowicz, J. *J. Power Sources* **1997**, *66*, 1−14.
(46) Kötz, R.; Carlen, M. *Electrochim. Acta* **2000**, *45*, 2483−2498.
(47) Shirley, D. A. *Phys. Rev. B* **1972**, *5*, 4709−4714.
(48) Spevack, P. A.; McIntyre, N. S. *J. Phys. Chem.* **1993**, *97*, 11031−11036.
(49) Swartz, W.; Hercules, D. M. *Anal. Chem.* **1971**, *43*, 1774−1779.
(50) Abdallah, W. e.; Nelson, A. E. *J. Mater. Sci.* **2005**, *40*, 2679−2681.
(51) Shenasa, M.; Sainkar, S.; Lichtman, D. *J. Electron Spectrosc. Relat. Phenom.* **1986**, *40*, 329−337.
(52) Yannopoulos, S. N.; Andrikopoulos, K. S. *J. Chem. Phys.* **2004**, *121*, 4747−4758.
(53) Müller, A.; Diemann, E.; Jostes, R.; Bögge, H. *Angew. Chem., Int. Ed.* **1981**, *20*, 934−955.
(54) Wang, H. W.; Skeldon, P.; Thompson, G. E.; Wood, G. C. *J. Mater. Sci.* **1997**, *32*, 497−502.
(55) Holleman, A. Fr.; Wiberg, E. *Lehrbuch der Anorganischen Chemie*; Walter de Gruyter: Berlin, 1985.
(56) Cotton, F. A.; Wilkinson, G.; Murillo, C. A.; Bochmann, M. *Advanced Inorganic Chemistry*, 6th ed.; Wiley-Interscience: New York, 1999.
(57) Srivastava, S. K.; Avasthi, B. N. *J. Mater. Sci.* **1993**, *28*, 5032−5035.
(58) Faraji, F.; Safarik, I.; Strausz, O. P.; Torres, M. E.; Yildirim, E. *Ind. Eng. Chem. Res.* **1996**, *35*, 3854−3860.
(59) Hu, K.; Hu, X.; Xu, Y.; Sun, J. *J. Mater. Sci.* **2010**, *45*, 2640−2648.
(60) Brito, J. L.; Ilija, M.; Hernández, P. *Thermochim. Acta* **1995**, *256*, 325−338.
(61) Bilal, B. A.; Tributsch, H. *J. Appl. Electrochem.* **1998**, *28*, 1073−1081.